Two-dimensional, two-electron model atom in a laser pulse: Exact treatment, single-active-electron analysis, time-dependent density-functional theory, classical calculations, and nonsequential ionization

D. Bauer

Theoretical Quantum Electronics (TQE), Technische Hochschule Darmstadt, Hochschulstrasse, 4A, D-64289 Darmstadt, Germany*

(Received 3 April 1997; revised manuscript received 27 May 1997)

Owing to its numerical simplicity, a two-dimensional two-electron model atom, with each electron moving in one direction, is an ideal system to study nonperturbatively a fully correlated atom exposed to a laser field. Frequently made assumptions, such as the ''single-active-electron'' approach and calculational approximations, e.g., time-dependent density-functional theory or (semi)classical techniques, can be tested. In this paper we examine the multiphoton short pulse regime. We observe ''nonsequential'' ionization, i.e., double ionization at lower field strengths as expected from a sequential, single-active-electron point of view. Since we also find nonsequential ionization in purely classical simulations, we are able to clarify the mechanism behind this effect in terms of single-particle trajectories. [S1050-2947(97)09509-7]

PACS number(s): 32.80.Rm

I. INTRODUCTION

Several theoretical approaches were able to reproduce experimentally observed ion yields in multielectron ionization, at least qualitatively (see, e.g. Ref. [1]). Most of them are based on a ''single-active-electron'' (SAE) point of view [2,3]. A new impact on the research in this field had the discovery of the so-called ''knee'' or ''shoulder'' in the ionization yields of helium exposed to a laser pulse [4]. This means that double ionization occurs *many orders of magnitude* more strongly at intensities where, according to a sequential SAE scenario, almost no He^{++} should be present. Early after the experimental observation of this nonsequential ionization (NSI), two possible mechanisms were suggested in order to explain it. Corkum proposed a rescattering scenario [5], where the first electron revisits the core and ionizes the second electron collisionally. Fittinghoff *et al.* suggested a ''shake-off'' effect [4] where the second electron ionizes due to the sudden loss of screening of the core by the first electron. Walker *et al.* [6] concluded by analyzing their experimental data that a rescattering process is not able to explain the observed yields. Their arguments are based on the absence of a rigorous threshold in the He^{++} yields. Instead they propose ''that NSI occurs via a simultaneous two-electron ejection either through a shake-off or threshold mechanism involving some form of electron correlation.'' Recently, the NSI mechanism has been clarified within the intense-field many-body S-matrix theory [7]. It was shown ''that the dominant mechanism behind the observed large probability of laser-induced double escape is a quantum-mechanical process of absorption of photon energy by one of the electrons which is shared cooperatively with the other electron through the Coulomb correlation.'' This mechanism for the NSI process was independently deduced from one-dimensional He studies, where the model atom had been exposed to a low frequency, short pulse laser field [8]: ''. . . before the outer electron disappears completely, the inner electron is already sufficiently strongly excited so that it leaves the atom within a short time interval later. It is during this time interval that the correlated double ionization takes place.'' Simulations where the outer electron is calculated in the SAE way but the inner one ''feels'' (in a second computer run) the time-dependent potential created by the outer one, succeeded in reproducing the NSI ''knee'' [9]. This result is also a strong indication that the suggested mechanisms as quoted above are, indeed, the correct ones. However, there is no detailed physical picture how this energy sharing between the outer and the inner electron takes place.

Our calculations were performed for a relatively high frequency ($\omega=0.4$ a.u.) and a very short pulse duration (six optical cycles) while in Ref. [8] a low-frequency short pulse was used. Since we are in the multiphoton regime rather than in the tunneling domain, the occurrence of NSI might be surprising. Indeed, in our calculations NSI is relatively weak compared to the many orders of magnitude effect for ionization of helium in strong low-frequency laser light. However, with the help of our additional classical simulations we are able to provide (i) a detailed physical picture how NSI takes place in terms of one-particle trajectories; and (ii) a proof that NSI, in its essence, is not a quantum mechanical effect.

Because the full quantum-mechanical numerical simulations of helium exposed to a laser field is an extremely demanding task [10], approximate approaches are desirable. Among these, Hartree-Fock [11–15], time-dependent density-functional theory (TDDFT) [16–19] and semiclassical molecular-dynamics calculations [20–23] are most frequently used. Especially the latter method succeeded in reproducing the ''knee'' [21]. On one hand, the molecular-dynamics calculations are very appealing and instructive since particle trajectories and single-particle energies can be traced. On the other hand, the additional ''Heisenberg force'' which must be introduced in order to avoid instabilities where one electron falls into the ''black hole'' (i.e., the nucleus) while the other one ionizes, is somewhat artificial and may evoke objections against the results produced by this method.

*URL: http://www.physik.th-darmstadt.de/tqe/

The time-dependent Hartree-Fock method was found to be problematic in the framework of multiphoton ionization [13–15]. Results from TDDFT, in principle an exact approach, depend on the choice of the effective exchange-correlation potential [24]. Another disadvantage of this procedure is that only the total electron density $n(\boldsymbol{r},t)=\Sigma_i|\varphi_i(\boldsymbol{r},t)|^2$ is calculated, and the single-particle orbitals $\varphi_i(\boldsymbol{r},t)$ are physically meaningless in a rigorous sense.

The study of systems where the motion of each electron is reduced to one spatial dimension has a relatively long tradition. Potentials of the form $-Z/\sqrt{x^2+\epsilon}$, so-called ''soft-core'' Coulomb potentials,'' provide an energetic Rydberg-like scaling [25] and lead to results qualitatively similar to those from full 3D calculations. Two 1D electrons are a two-dimensional system which is tractable with computers nowadays. Two 1D electron system are used to study nonperturbatively autoionization [26], ionization of a negative ion [27], validity of time-dependent Hartree-Fock theory for the multiphoton ionization of atoms [13–15], and, most recently, two-electron effects in harmonic generation and ionization [8].

This paper is organized as follows. In Sec. II, the model system is introduced. In Sec. III results from the 2D quantum calculations are presented. Section IV is devoted to an analysis of the results in terms of a SAE approach. In Sec. V we present results from a time-dependent density-functional calculation, and in Sec. VI we discuss our classical particle simulations within which the NSI scenario can be clarified. Finally, we summarize and conclude in Sec. VII.

II. 1D HELIUM MODEL

The two 1D electrons with coordinates x and y interact with the core and with each other through a ''soft-core'' interaction, i.e., $-2/\sqrt{x^2+\epsilon}$ and $1/\sqrt{(x-y)^2+\epsilon}$, respectively, and with the field $E(t)$ through the dipole term $(x+y)E(t)$ [atomic units (a.u.) will be used throughout this paper]. Thus the total Hamiltonian reads

$$H(x,y,t)=-\frac{1}{2}\frac{\partial^2}{\partial x^2}-\frac{1}{2}\frac{\partial^2}{\partial y^2}-\frac{2}{\sqrt{x^2+\epsilon}}-\frac{2}{\sqrt{y^2+\epsilon}}+\frac{1}{\sqrt{(x-y)^2+\epsilon}}+(x+y)E(t). \quad (1)$$

The desired ground-state energy can be tuned by varying ϵ. We used

$$\epsilon=0.55$$

in our calculations, which leads to the ground-state energy

$$\varepsilon_0=-2.897 \text{ a.u.}$$

on our numerical grid. ε_0 is approximately the ground-state energy for the real 3D helium atom which is -2.902.

One may prefer thinking in terms of *one 2D particle* which moves in the somewhat peculiar 2D potential,

$$V(x,y,t)=-\frac{2}{\sqrt{x^2+\epsilon}}-\frac{2}{\sqrt{y^2+\epsilon}}+\frac{1}{\sqrt{(x-y)^2+\epsilon}}+(x+y)E(t), \quad (2)$$

instead of the two electrons interacting with each other. Potential (2) and the ground-state energy level are shown in Fig. 1 for the three constant fields $E=0.0$, 0.1, and 0.616. The electric field E tilts the field-free potential around the axis $y=-x$.

In order to estimate at what field strengths strong single and double ionization should occur, it is advantageous to calculate the classical critical fields. However, the commonly used method of equating the initial ground-state energy level to the maximum of the barrier formed by the atomic potential and the external field leads to an unphysically small critical field $E^{+}_{\text{crit}}=0.009$ for single ionization. In our numerical simulations in the next sections we will find a negligible ionization probability for such low-field strengths. As in the case of hydrogenlike ions, the electron is not able to move beyond the point where the energy level touches the lowest point of the energetic barrier [28]. Therefore the ''real'' critical field is higher. On the other hand, total ionization should be strong at the latest when the ground-state energy level exceeds the electron-electron repulsion ridge in the $x=y$ direction. This is the case at $E^{++}=0.616$ [see Fig. 1(c)].

III. QUANTUM CALCULATION

We used a spectral method [29] to solve the time-dependent Schrödinger equation

$$i\frac{\partial}{\partial t}\Psi(x,y,t)=H(x,y,t)\Psi(x,y,t),$$

with the Hamiltonian (1). In order to keep the numerical effort as small as possible we chose a rather high laser frequency

$$\omega=0.4,$$

and a very short pulse covering six cycles,

$$T=6\frac{2\pi}{\omega}=94.248.$$

The pulse envelope was $\sin^2$ shaped, thus

$$E(t)=\hat{E}\,\sin^2\left(\frac{\pi}{T}t\right)\sin\omega t \quad (3)$$

for $0<t<T$. With the frequency chosen and $\hat{E}$ not greater than 1, we are in the multiphoton domain, since the Keldysh parameter $\sqrt{|\varepsilon_0|/(2U_p)}$ is not much less than unity over the whole intensity region of interest. U_p is the ponderomotive potential $\hat{E}^2/(4\omega^2)$, i.e., the mean quiver energy of a free electron in the laser field. A spatial grid spacing $\Delta x=\Delta y=0.4$ and a temporal one $\Delta t=0.1$ was found to be sufficient. We chose the grid size large enough so that almost no probability density reaches the boundaries within the pulse time T. The ground-state wave function was determined by propa-

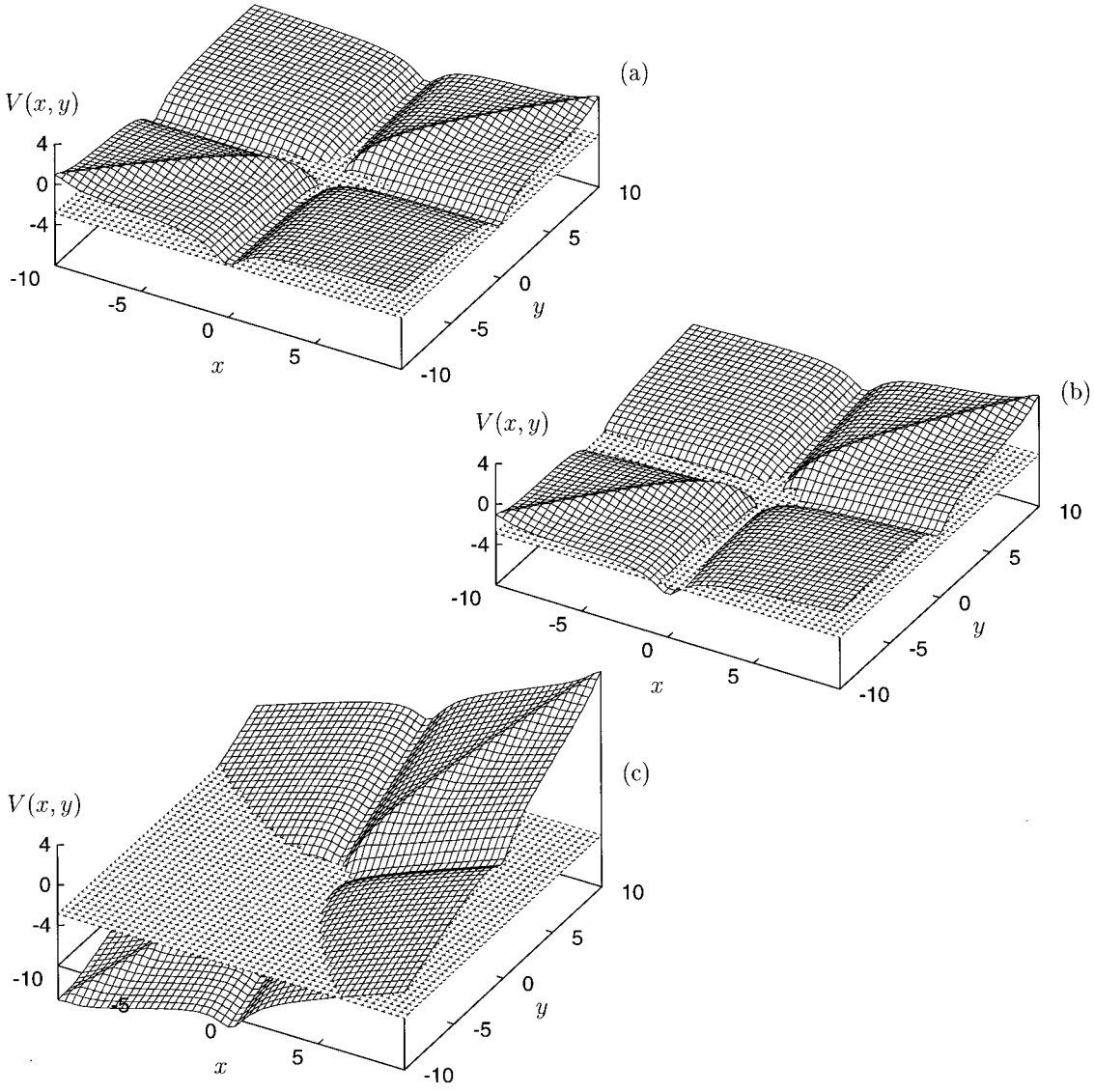

FIG. 1. The 2D potential $V(x,y)$ (2) for $\hat{E}=0.0$, (a), $\hat{E}=0.1$ (b), and $\hat{E}=0.616$ a.u. (c). At $\hat{E}=0.1$ the initial ground-state level cuts the effective potential within the single-ionization channels. For $\hat{E}=0.616$ the ground state level even exceeds the potential ridge along $x=y$. At that field strength strong double ionization is expected.

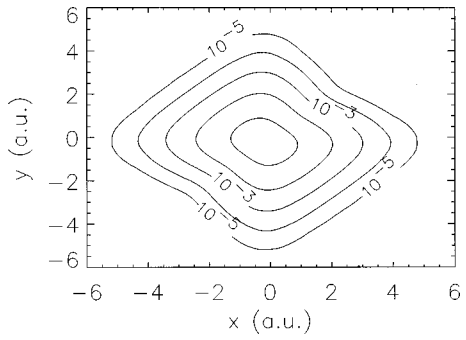

FIG. 2. Contour plot of the ground-state probability density. The energy is $\varepsilon_0=-2.897$. The electron-electron repulsion along $x=y$ clearly leaves its fingerprint on the wave function (butterfly shape). Such an asymmetric shape is absent in corresponding Hartree–Fock [14] or simple DFT ground states.

gating a Gaussian seed function in imaginary time. A contour plot of the ground-state probability density is shown in Fig. 2. Its energy is $\varepsilon_0=-2.897$.

If we assume that one electron is already ionized, we are left with the 1D version of hydrogenlike helium He^+. The ground-state energy of this system,

$$i\frac{\partial}{\partial t}\Psi^+(x,t)=\left(-\frac{1}{2}\frac{\partial^2}{\partial x^2}-\frac{2}{\sqrt{x^2+\epsilon}}\right)\Psi^+(x,t), \qquad (4)$$

was determined to be $\varepsilon^+=-1.920$. Therefore, the ionization energy for the ''outer'' electron is $\varepsilon_0-\varepsilon^+=-0.977$. The removal energy for the outer electron in real 3D He is 0.9 a.u.

The probability density $|\Psi(x,y,t)|^2$ during the pulse for the peak field strength $\hat{E}=0.3$ is shown in Fig. 3. One looks

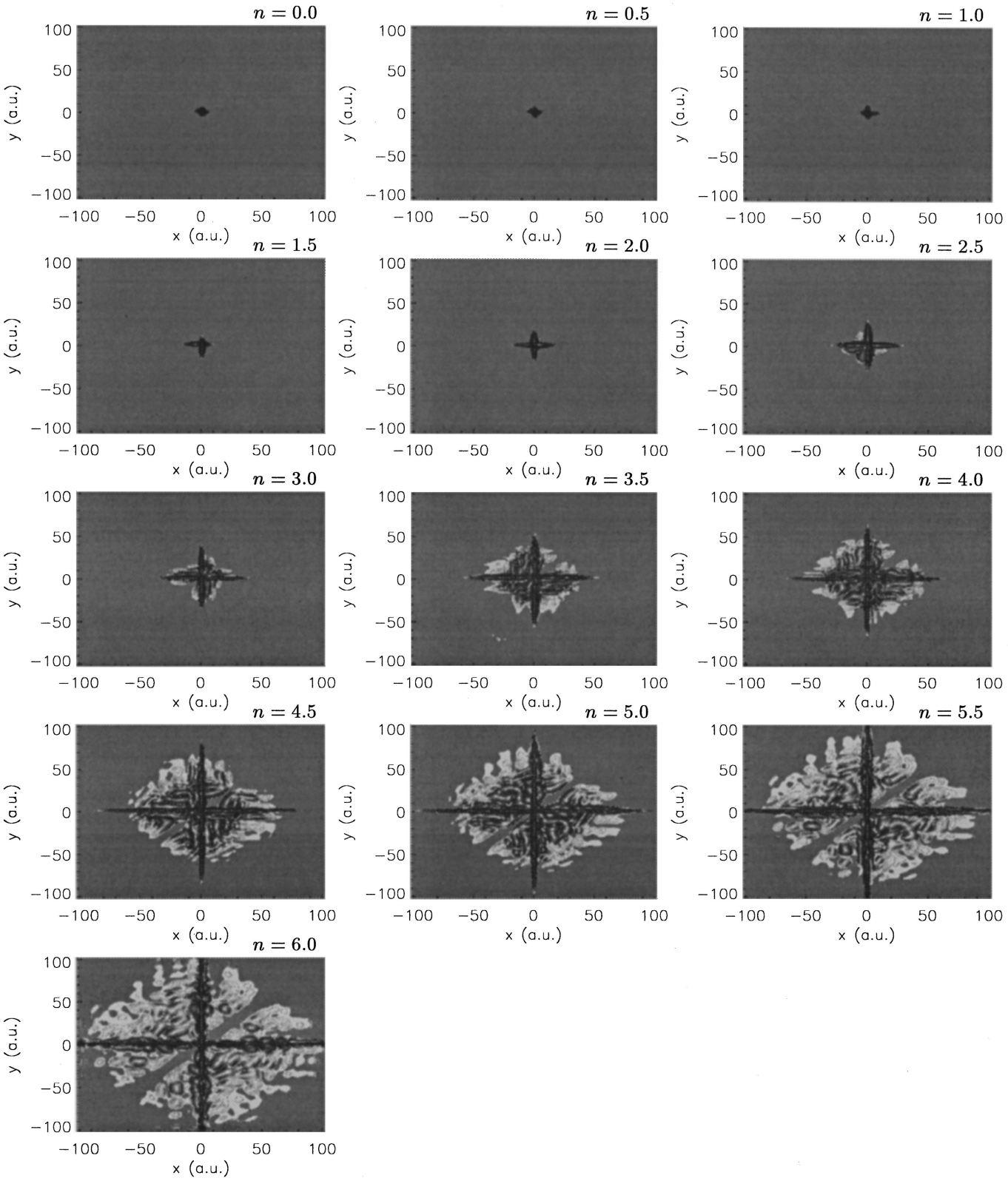

FIG. 3. The probability density after n optical cycles for $\hat{E}=0.3$ a.u. One looks perpendicularly from above onto the illuminated xy plane and the logarithmically scaled probability density $|\Psi(x,y,t)|^2$. Up to $n=2$, mainly single ionization takes place (the probability density is along the axes). Afterwards regions $|x|,\ |y|>5$ also are occupied, which corresponds to double ionization. The Coulomb-repulsion ridge along $y=x$ can be clearly identified at later times.

perpendicularly from above onto the illuminated, logarithmically scaled probability density.

Density flowed along the $\pm x$ or $\pm y$ axis corresponds to single ionization, while double ionization occurs when both $|x|$ and $|y|$ are significantly greater than the width of the ground state. We use this simple picture to define our ionization probabilities at the end of the laser pulse for total, double, and single ionization P, P^{++}, and P^{+}, respectively:

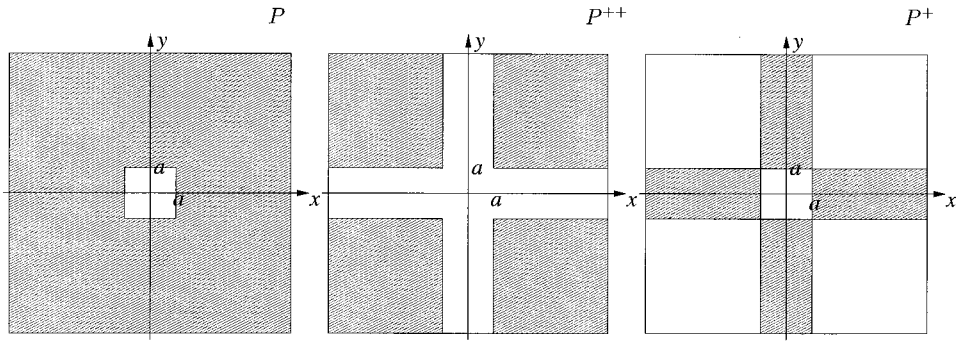

FIG. 4. The areas to be integrated over in order to calculate the probabilities for (from left to right) total, double, and single ionization are shaded. The parameter a was chosen to be 5 a.u.

$$P=1-\int_{-a}^{a}\int_{-a}^{a}|\Psi(x,y,T)|^2dx\ dy, \tag{5}$$

$$P^{++}=1-\int_{-\infty}^{\infty}\int_{-a}^{a}|\Psi(x,y,T)|^2dx\ dy - \int_{-a}^{a}\int_{-\infty}^{\infty}|\Psi(x,y,T)|^2dx\ dy + \int_{-a}^{a}\int_{-a}^{a}|\Psi(x,y,T)|^2dx\ dy, \tag{6}$$

$$P^{+}=P-P^{++}. \tag{7}$$

We chose $a=5$. In Fig. 4 the integration areas corresponding to P, P^{++}, and P^{+} are shown.

Of particular interest is the evolution of the probability density when the double-ionization regions $|x|>5$ *and* $|y|>5$ are occupied for the first time. In Figs. 5 and 6 these time intervals are shown for $\hat{E}=0.2$ and 0.7, respectively. The delay between the snapshots is a quarter optical cycle in each case.

Let us first analyze the $\hat{E}=0.2$ case in Fig. 5. Till $n=2.75$ optical cycles mainly single ionization has occurred, i.e., the probability density is still located along the axes. At time $n=3.00$ two density jets enter the region $x,\ y>0$ (indicated by two arrows). They are clearly separated by the Coulomb repulsion ridge along $y=x$. These density jets represent states where both electrons are on the same side of the nucleus. Therefore the Coulomb repulsion is relatively high, and the jets tend to flow back toward the single-ionization channels. This reflux of probability density is supported by the electric field which has its maximum a quarter of a cycle later, at $n=3.25$. However, some density passes the single ionization channels and appears in the regions $x>0,\ y<0$ and $x<0,\ y>0$, respectively (see arrows in the $n=3.25$ and $n=3.5$ plots). Now the two electrons represented by this density are on opposite sides of the nucleus, and both are ionized. So we conclude that although the electric-field amplitude $\hat{E}$ is not sufficiently strong to double ionize by simply tilting the xy plane, Coulomb repulsion *and* electric field can lead to double ionization by acting together constructively. Therefore we propose *Coulomb-repulsion-assisted laser acceleration* to be responsible for NSI.

At higher intensities ($\hat{E}=0.7$, Fig. 6) we also observe the two density jets entering regions of the xy plane, where x and y have equal signs (see $n=2.00$ till $n=2.25$). However, reflux of these jets is obviously not essential to stimulate subsequent emission of the probability density into regions $x>0,\ y<0$ and $x<0,\ y>0$, respectively. This can be seen in the plot $n=2.25$, where already bursts of density leave the single ionization channels although the jets are not yet flown back. Here double ionization is mainly due to the strongly tilted xy plane.

Note that these backflowing jets which support double ionization are of course absent in the SAE model, while they are expected to be included in TDDFT, since there both electrons are allowed to respond to the field simultaneously. Furthermore, purely classical simulations should show a similar NSI scenario as the quantum density current in the xy plane, i.e., electrons which collide while moving in the same direction (the two jets) followed by a subsequent turn of one electron which crosses the origin and finally leaves in the opposite direction. All these presumptions will be confirmed in the next sections.

We performed several runs varying the peak field strength $\hat{E}$. In Fig. 7 the ionization degrees P, P^{+}, and P^{++} are plotted vs the intensity $I=\hat{E}^2$. There are also shown the ionization probabilities P_{sequ} and PP_{sequ}, which result from solving Eq. (4) in the external laser field. As long as P^{++} is small, PP_{sequ} would be the probability for He^{++} production if double ionization occurs purely sequentially, i.e., the first electron no longer interacts with the residual ion, and the second electron remains nonexcited after the emission of the first one. Obviously this completely sequential scenario cannot explain the correct ionization degree P^{++}. Double ionization occurs earlier than predicted by PP_{sequ}. This corresponds to the experimentally observed ''knee'' in the He-ion yields, although our He^{++} curve does not show such a pronounced shape due to the fact that we are in the multiphoton regime and not in the tunneling regime as in Ref. [8]. We also performed some runs using $\omega=0.2$, and saw an increasing deviation from the SAE He^{++} curves, i.e., an increasing ''knee.'' The P_{sequ} and PP_{sequ} curves cross the correct P^{++} result, since depletion of the He^{+} ions is not taken into account.

IV. SINGLE ACTIVE ELECTRON ANALYSIS

In Sec. III we already compared the correct ionization degree P^{++} with the product PP_{sequ} for the rate when the second electron ionizes from its He^{+} ground state without interacting with the electron already freed. The ionization degree PP_{sequ} was found to be too small in the intensity

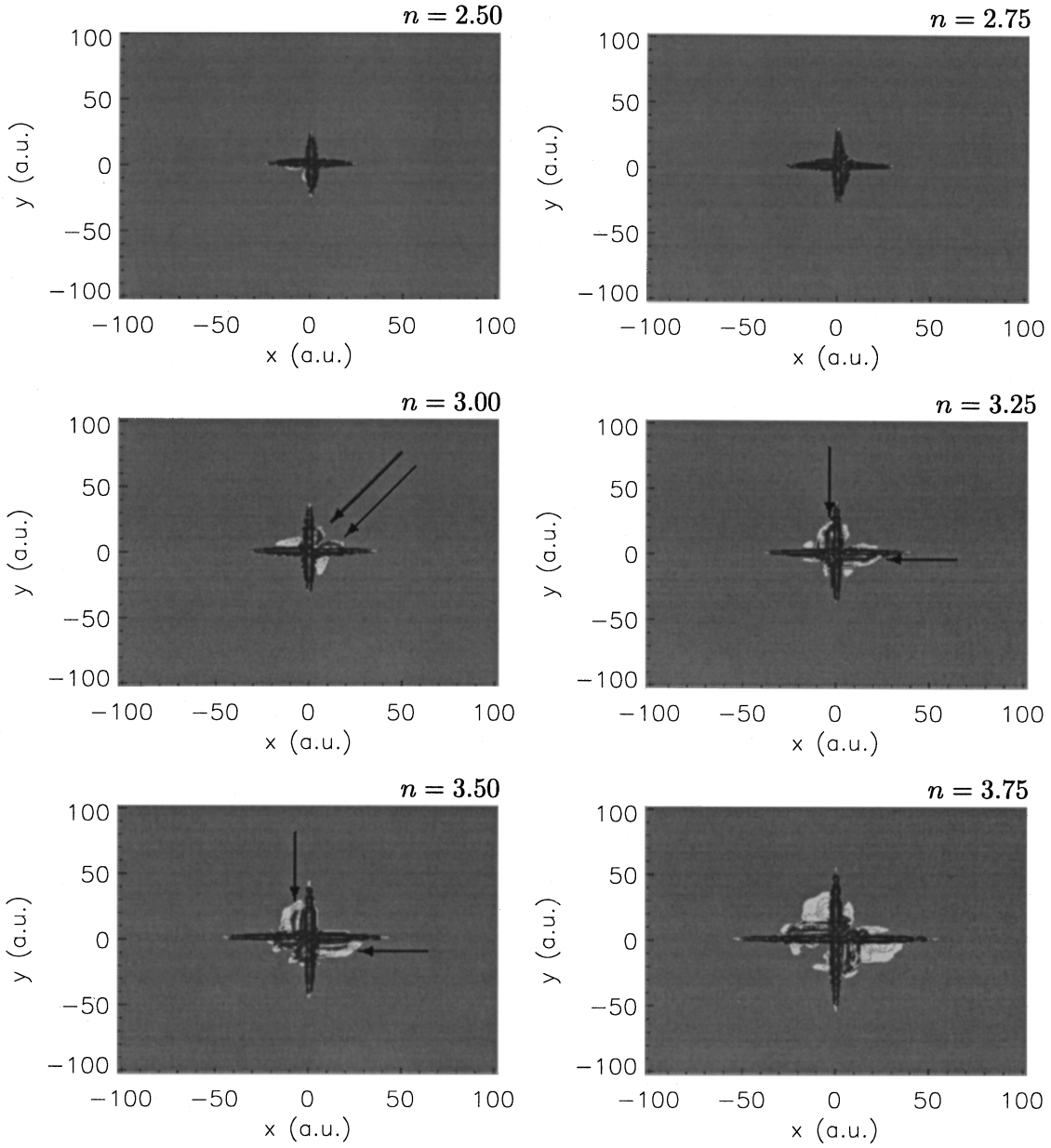

FIG. 5. The probability density for $\hat{E}=0.2$ a.u. at $n=2.5$, 2.75, 3, 3.25, 3.5, and 3.75 optical cycles. At time $n=3$ two probability density jets are emitted into the region $x,y>0$. At $n=3.25$ they are partly flown back and density appears in regions $x<0$, $y>0$, and $y<0$, $x>0$.

region of interest $0.02<I<0.07$, as depicted in Fig. 7.

Now we may try to describe the ionization probability P^+ in the single-active-electron approach. In order to do this we have to find an appropriate Z_{eff}, and to solve the equation

$$i\frac{\partial}{\partial t}\Psi^0(x,t)=\left(-\frac{1}{2}\frac{\partial^2}{\partial x^2}-\frac{Z_{\text{eff}}}{\sqrt{x^2+\epsilon}}\right)\Psi^0(x,t). \qquad (8)$$

The first electron has an ionization potential $\varepsilon_0-\varepsilon^+=-0.977$. We found that $Z_{\text{eff}}=1.117$ yields such a binding energy. In Fig. 8 the ion yields $\tilde{p}^+$ which result from solving Eq. (8) in the external field are shown and computed with the exact result p^+. The ionization degree $\tilde{p}^+$ is too high over the whole region, where mainly single ionization takes place. As soon as double ionization occurs, the curve also differs qualitatively from the exact one: there is a dip in the exact P and P^+ curves around $I=0.03$, which is absent in the $\tilde{P}^+$ result. We conclude that the second electron shares some energy with the escaping first electron which leads to a decreased single-ionization probability. Since in a similar work for a very low frequency [8] the SAE curves are found to fit well, the deviations we observe might be mainly due to the relatively high frequency we have chosen. For higher frequency laser fields the ''cracking up'' of the initial ground-state wave function into ''inner'' and ''outer'' electrons may be too slow to be well described by an SAE ansatz for the ''outer'' electron.

One may object that, although tuning Z_{eff} in order to fit the binding energy of the ''outer'' electron leads to an overestimation of the ion yields, there might be a certain combination of Z_{eff} and an effective soft-Coulomb parameter ϵ_{eff}

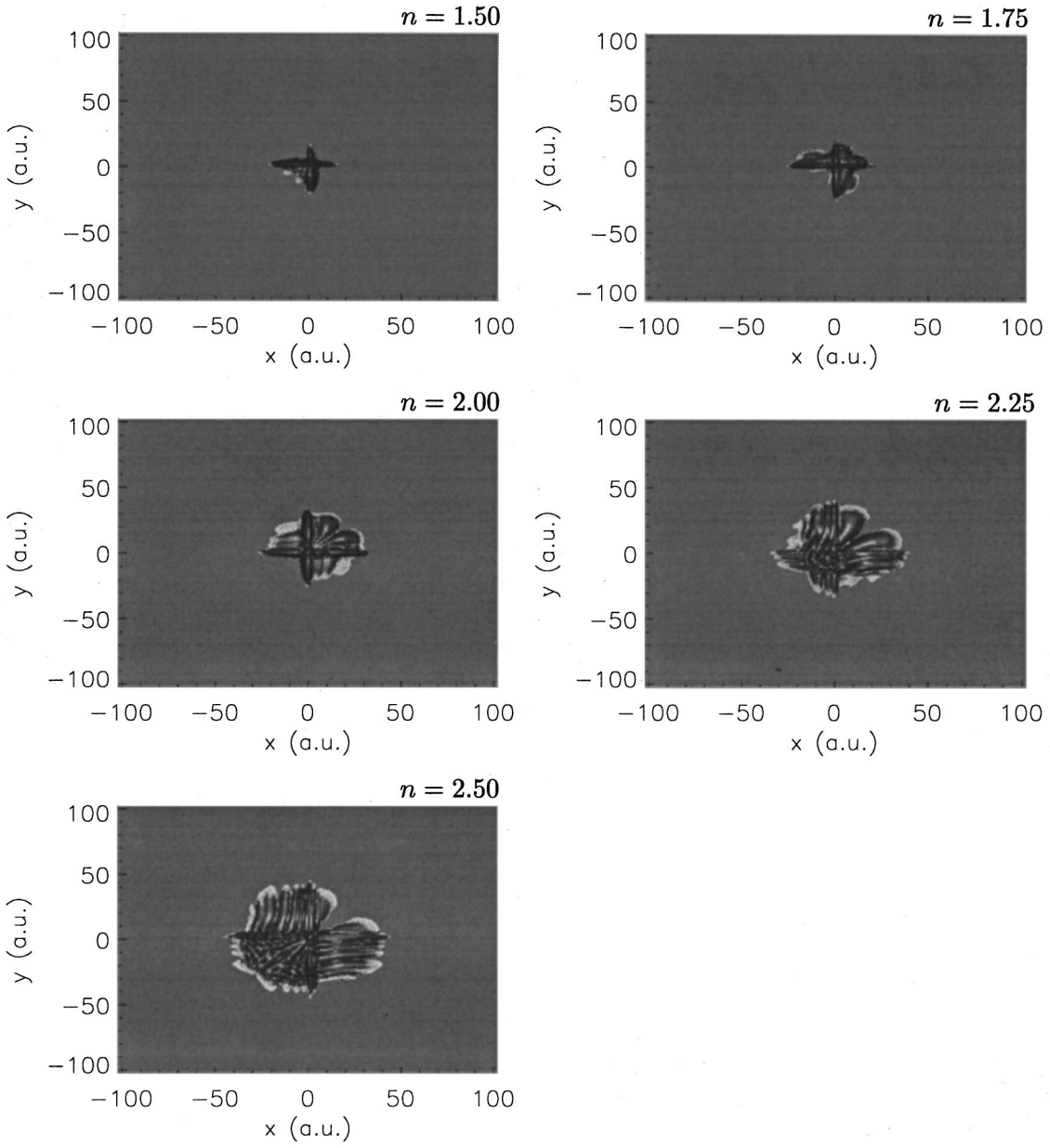

FIG. 6. The probability density for $\hat{E}=0.7$ a.u. at $n=1.5$, 1.75, 2, 2.25, and 2.5 optical cycles. Double ionization is mainly due to the strongly tilted xy plane.

which does both: providing the correct binding energy *and* the right ionization probabilities. However, we tried $Z_{\mathrm{eff}}=1$ and $\epsilon_{\mathrm{eff}}=0.398$, which also led to the desired binding energy -0.977. The resulting curve for the single ionization yields are also shown in Fig. 8. It overestimates the single ionization as well.

V. DENSITY-FUNCTIONAL THEORY

Density-functional theory is a powerful tool in determining multielectron atomic structures (see, e.g., Refs. [16,30] for an overview). It has been shown [31] that a Hohenberg-Kohn-type theorem also exists for time-dependent phenomena. Therefore the existence of an effective potential which transforms the problem of N interacting electrons to that of N noninteracting ones is proved. The noninteracting electrons move in an effective potential which is a functional of

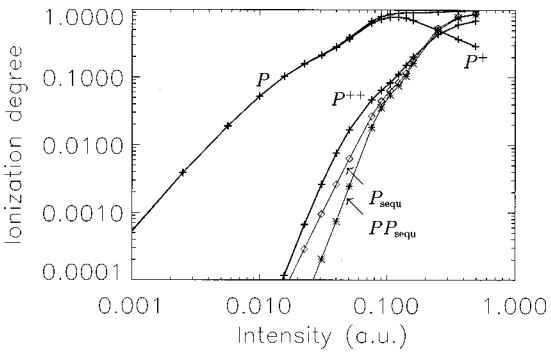

FIG. 7. The 2D calculation results for total, single, and double ionization (bold, +). The SAE result for the $He^{+}\rightarrow He^{++}$ is also drawn ($\diamond$). Multiplication with P (see text) leads to the expected sequential double-ionization degree (*) as long as $P^{++}\ll P^{+}$. The P_{sequ} and PP_{sequ} curves intersect the correct P^{++} results since depletion of the He^{+} ions is not taken into account.

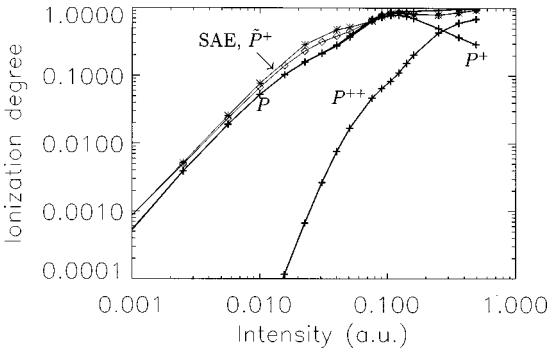

FIG. 8. SAE results for the outer electron compared with the exact 2D yields (bold,+). The curve plotted with connected * was calculated using $Z_{\rm eff}=1.117$ and $\epsilon_{\rm eff}=0.55$. For the $\diamond$ curve $Z_{\rm eff}=1$, $\epsilon_{\rm eff}=0.398$ was chosen. In both cases the SAE ionization degrees are too high.

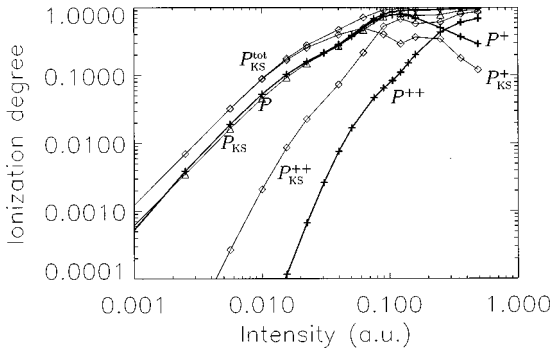

FIG. 9. Comparison of the TDDFT results with the exact 2D solutions. The total ionization degrees $P_{\rm KS}$ ($\triangle$) matches nicely the exact curve (bold,+). If one claims physical relevance for the Kohn–Sham orbitals, one obtains $\diamond$ curves for $P^{\rm tot}_{\rm KS}$ (total), $P^{+}_{\rm KS}$ (single) and $P^{++}_{\rm KS}$ (double) ionization, which agree poorly with the exact probabilities (see the text for a discussion).

the total electron density only. The problem reduces to finding an appropriate effective potential which includes all relevant exchange and correlation effects. There is some recent work on the field of TDDFT applied to laser ionization of atoms [16–19].

In the case of a singlet two-electron system like our model atom of helium, there is only one occupied Kohn-Sham orbital $\varphi(x,t)$. The total electron density is

$$n(x,t)=2|\varphi(x,t)|^2. \tag{9}$$

There are no exchange contributions, and neglecting correlation effects leads to the time-dependent Hartree equation

$$i\frac{\partial}{\partial t}\varphi(x,t)=\left(-\frac{1}{2}\frac{\partial^2}{\partial x^2}-\frac{2}{\sqrt{x^2+\epsilon}}+\int\frac{|\varphi(x',t)|^2}{\sqrt{(x-x')^2+\epsilon}}dx'+xE(t)\right)\psi(x,t). \tag{10}$$

Hartree's independent electron-model was already used by Geltman in 1985 to analyze experimental results in the multiple ionization of atoms [32,33].

The ground-state energy we obtained by solving Eq. (10) in imaginary time is $\varepsilon^0_{\rm KS}=-2.878$.

In Fig. 9 the comparison between the TDDFT results and the exact ones are made. The ionization yields for He^+ and He^{++} are observables, of course. Thus they are functionals of the density $n(x,t)$ and, due to the simple relation (9), explicit functionals of the Kohn-Sham-orbital density $|\varphi(x,t)|^2$. We want to adopt the simple ''integration-over-areas'' picture in order to calculate the ionization, as described in Sec. III. According to Ref. [18], we proceed, for the time being, as follows: with

$$P_{\rm KS}:=1-\int_{-a}^{a}|\varphi(x,t)|^2dx, \tag{11}$$

the probability for neutral helium is the product of the probabilities for each orbital to be nonionized. Thus

$$P^0_{\rm KS}=(1-P_{\rm KS})^2. \tag{12}$$

For the single and double ionization

$$P^+_{\rm KS}=2P_{\rm KS}(1-P_{\rm KS}), \tag{13}$$

$$P^{++}_{\rm KS}=P^2_{\rm KS} \tag{14}$$

follows, and the total ionization clearly is

$$P^{\rm tot}_{\rm KS}=1-P^0_{\rm KS}. \tag{15}$$

The three curves corresponding to $P^{\rm tot}_{\rm KS}$, $P^+_{\rm KS}$, and $P^{++}_{\rm KS}$ are shown in Fig. 9. The agreement is quite bad. The total- and single-ionization degrees are overestimated as in the SAE calculation.

However, the total ionization $P_{\rm KS}$ fits the exact P well if one avoids assigning any physical relevance to the Kohn-Sham orbital $\varphi(x,t)$ and proceeds instead as follows: $P_{\rm KS}$ as defined in Eq. (11) is the probability to find *any* of the two electrons outside the interval $[-a,a]$, since the *physical* total electron density is $n(x,t)=2|\varphi(x,t)|^2$. Therefore the probability for total ionization should be simply

$$P^{\rm tot}_{\rm KS}=P_{\rm KS}, \tag{16}$$

and

$$P^0_{\rm KS}=1-P_{\rm KS}.$$

$P^{\rm tot}_{\rm KS}$, according Eq. (16), is also depicted in Fig. 9. The agreement between $P_{\rm KS}$ and P is excellent. The dip around $I=0.03$ is well reproduced. Since the dip is absent in the SAE results, the onset of NSI seems to be included in the TDDFT, although only the simple Hartree effective potential is taken.

There is no simple way to deduce $P^+_{\rm KS}$ and $P^{++}_{\rm KS}$ without claiming physical significance of the Kohn-Sham orbital $\varphi(x,t)$, although the *existence* of purely density-dependent functionals $P^+_{\rm KS}[n]$ and $P^{++}_{\rm KS}[n]$ are proved by the Hohenberg-Kohn theorem. Equations (12)–(15) would be valid if the correct wave function $\Psi(x,y,t)$ was the product of the Kohn-Sham orbitals, $\varphi(x,t)\varphi(y,t)$. A plot of

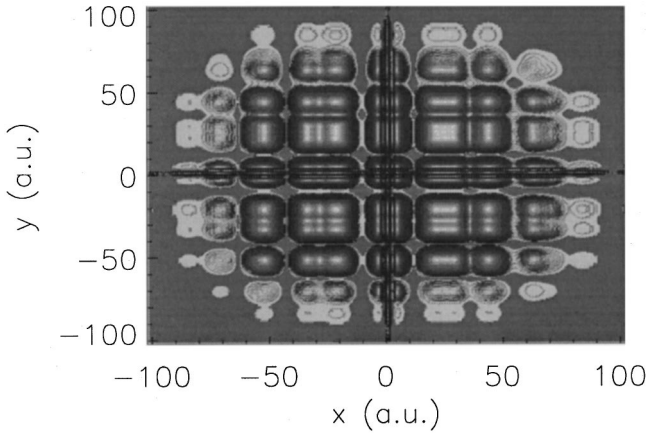

FIG. 10. The TDDFT probability density at the end of the pulse for $\hat{E}=0.3$ a.u. The gridlike pattern is due to the construction as a pure product of the Kohn-Sham orbitals. There is no displacement of probability density along $y=x$, of course.

$|\varphi(x,T)|^2|\varphi(y,T)|^2$ for $\hat{E}=0.3$ is shown in Fig. 10. Clearly, there is a gridlike pattern imprinted due to the construction of the wave function as a pure product. This leads to a totally different angular distribution in the xy plane. A similar behavior is observed in time-dependent unrestricted Hartree-Fock calculations [15].

However, for higher field strengths both electrons are ionized rapidly, and subsequently behave as free and almost independent electrons. Thus the total wave function should develop a gridlike pattern. This is shown in Fig. 11, where the peak field strength $\hat{E}=0.7$ is chosen. The TDDFT result is also plotted.

VI. CLASSICAL SIMULATIONS

We solved the classical equations of motion according the Hamiltonian (1) and the electric field (3) for a microcanical ensemble of the two electrons. We traced the one-particle energies

$$\varepsilon_x(x,y)=\tfrac{1}{2}\dot{x}^2-\frac{2}{\sqrt{x^2+\epsilon}}+\frac{1}{\sqrt{(x-y)^2+\epsilon}}, \tag{17}$$

$$\varepsilon_y(x,y)=\tfrac{1}{2}\dot{y}^2-\frac{2}{\sqrt{y^2+\epsilon}}+\frac{1}{\sqrt{(x-y)^2+\epsilon}}. \tag{18}$$

The total energy is

$$\varepsilon(x,y,t)=\varepsilon_x(x,y)+\varepsilon_y(x,y)-\frac{1}{\sqrt{(x-y)^2+\varepsilon}}+(x+y)E(t).$$

Each electron is considered to be ionized when $\varepsilon_x(x,y)>0$ or $\varepsilon_y(x,y)>0$, respectively. There is no unique way in defining the single-particle energies (17) and (18) since the electron-electron term may be shared between the two electrons in various ways [20]. However, this has little influence on the ionization degrees since, in the case of single or double ionization, the distance between the two electrons is normally large at the end of the pulse.

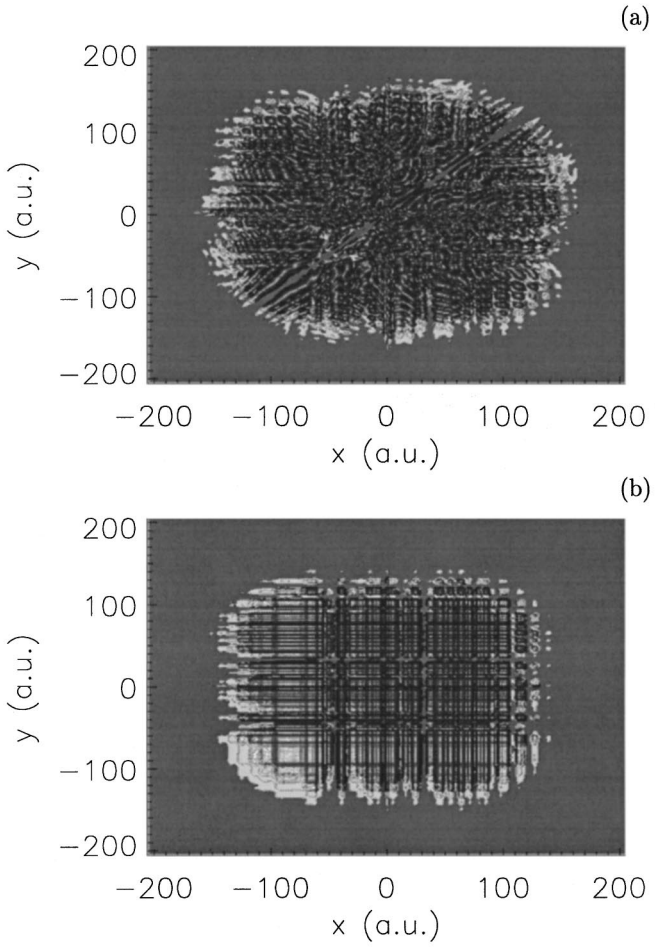

FIG. 11. The probability densities at the end of the laser pulse for $\hat{E}=0.7$ a.u. In plot (a) the exact density is presented, and (b) the TDDFT result is presented. The exact density (a) develops a gridlike pattern since both electrons were ionized rapidly and subsequently behaved like almost free electrons, i.e., the wave function becomes more and more a pure product of single-particle wave functions. However, the agreement with the product of the Kohn-Sham orbitals, (b) is poor even at those high-field strengths.

The initial conditions were chosen to meet the quantum mechanical ground-state energy $\varepsilon_0=-2.897$. Fortunately, the resulting ion yields were not sensitive to the choice of the ensemble of initial conditions. Instead of taking several initial positions and momenta, we started with one ''mother'' configuration at $t=0$ and varied the time $t_{\rm on}$ where the laser pulse sets in. We tried several mother configurations to ensure insensibility of the resulting ion yields. We would like to mention that a classical treatment of a 1D model helium has also been undertaken in Ref. [34] in the framework of stabilization of multielectron atoms.

The results are shown in Fig. 12. The single ionization is strongly overestimated. This is due to the fact that the ionizing electron gains energy at the expense of the still bound electron which occupies a state of quantum-mechanically forbidden low energy, i.e., an energy below -1.920. This is shown in Fig. 13 where the two one-particle-energies ε_x and ε_y are plotted for a representative single-ionization event at $\hat{E}=0.1$.

This behavior could be prevented if one introduces a

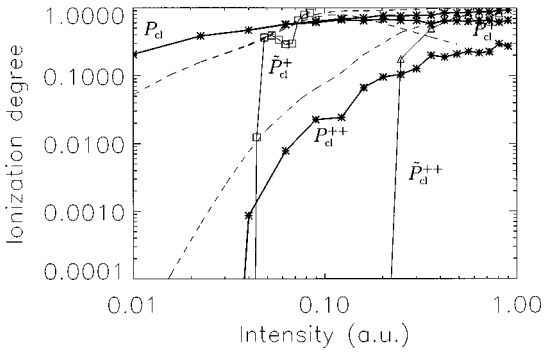

FIG. 12. The classical yields (bold,*) for P_{cl} (total), P^{+}_{cl} (single) and P^{++}_{cl} (double) ionization. The single ionization is strongly overestimated (compare with the exact quantum-mechanical results, drawn dashed) due to the classical effect discussed in the text. The classical SAE results for the outer ($\tilde{P}^{+}_{cl}$, $\Box$) and the inner electron ($\tilde{P}^{++}_{cl}$, $\triangle$) are also plotted. There is classical NSI at $I=0.04$ even when no sequential single ionization should occur.

velocity-dependent ''Heisenberg'' potential [20]. However, for our purpose of studying the NSI mechanism this is not necessary. We have calculated also the classical SAE single-ionization process in the potential $V(x)=-Z_{\rm eff}/\sqrt{x^2+\epsilon}$ with $Z_{\rm eff}=1.117$ as in Sec. IV. The resulting yields are lower, and show a rapid increase at the critical intensity which is 0.05 for the potential used. This is the typical behavior in pure classical simulations. Note that double ionizations is already observed where, according to the SAE approach, not even classical single ionization occurs.

The result of the SAE calculation $He^{+}\rightarrow He^{++}$ was multiplied with the probability for He^{+} production from the full 2D run. Below $I=0.25$, the classical critical intensity for sequential He^{++} production the probability vanishes, as expected. Thus the intensity region $0.03<I<0.2$ is the classical NSI regime we are particularly interested in. We examined each double-ionization event in that region. The ionization

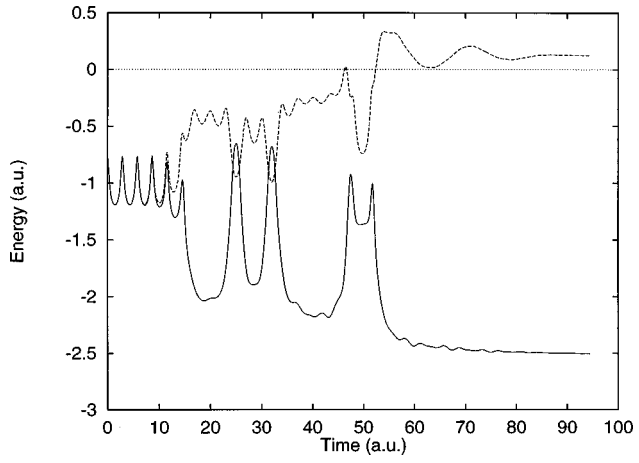

FIG. 13. A representative example for classical single ionization in terms of the single-particle energies (17) and (18). The inner electron (solid) drops below the quantum-mechanical He^{+} binding energy -1.920. This leads to an overestimation of the single-ionization probability since the outer electron (dashed) can gain more energy during Coulomb collisions (see peaks in the energy curves) with the inner electron as allowed quantum mechanically.

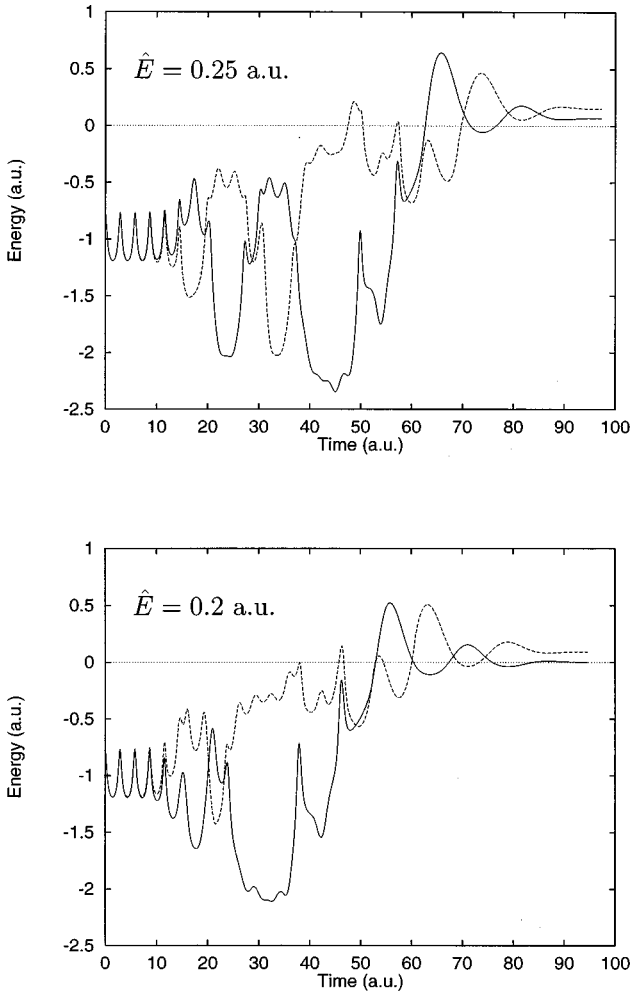

FIG. 14. Two representative classical NSI scenarios in terms of the single-particle energies (17) and (18).

dynamics of two representative examples in terms of single-particle energies and trajectories is depicted in Figs. 14 and 15.

For the purpose of comparing our classical results with the quantum-mechanical probability density current in the xy plane, we look at the electron trajectories in Fig. 15. One observes that the electron which leaves first is accompanied by the other electron moving in the same direction (corresponding to density flowing into regions of the xy plane, where x and y have equal sign). The Coulomb interaction is strong within that half-cycle. Then, as the first electron ionizes, the second one turns around and moves in the opposite direction (corresponding to probability density passing one of the xy plane's axes). Thus the second electron in NSI leaves the atom approximately one-half laser cycle after the first one. The dynamics of the classical test particles corresponds to the temporal and spatial evolution of the quantum probability density as described in Sec. III.

In Fig. 16 we show a representative example for double ionization at a higher field strength ($\hat{E}=1.0$). At this field strength the sequential pathway is more probable than NSI. The temporal delay between the ionization of the two electrons is greater (1–3 cycles) but still small, since our pulse is ramped strongly over three cycles only. In longer pulses the temporal delay between the ejection of the two electrons would be even greater.

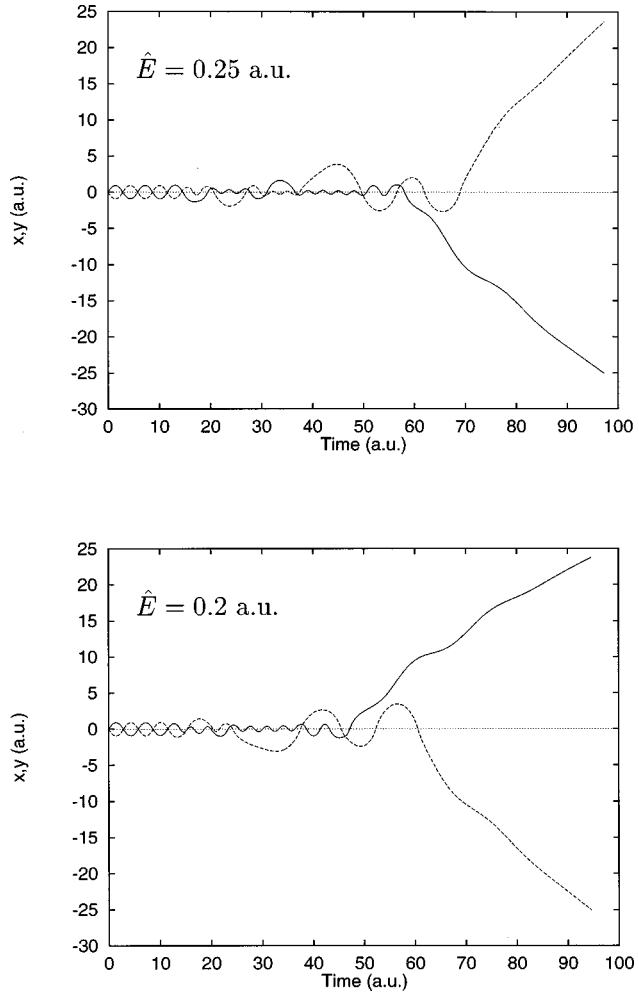

FIG. 15. The particle trajectories corresponding to Fig. 14. The electrons become free within approximately one-half an optical cycle. Before both electrons ionize they move together in the same direction for a quarter of a cycle until one electron turns and finally vanishes in the opposite direction. This has to be compared with the quantum dynamics in Fig. 5.

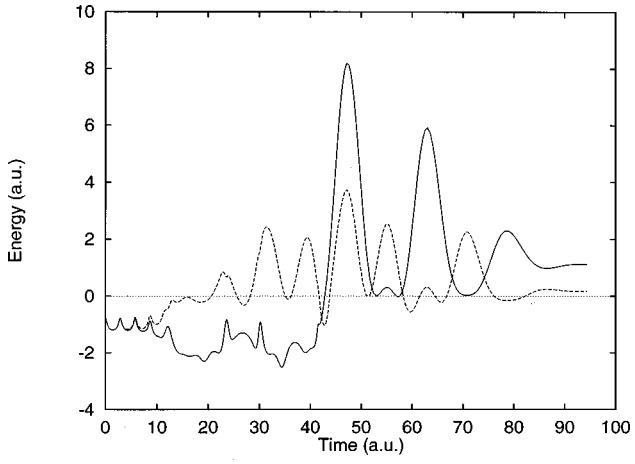

FIG. 16. A representative example of classical sequential double ionization at $\hat{E} = 1.0$ a.u. The temporal delay between the ejection of the two electrons is three half-cycles, and would be even greater in a more adiabatically ramped pulse.

VII. CONCLUSIONS

In this paper we have confirmed the recently proposed mechanism for the NSI process, namely, the ionization of the second electron by Coulomb interacting with the outer partner. We have traced the NSI scenario by observing the quantum-mechanical probability density as it evolves in space and time. We have identified the *Coulomb-repulsion-assisted laser acceleration* of the inner electron to be responsible for NSI. Our classical simulations have supported this point of view and contributed to a detailed picture of how NSI happens in terms of one-particle energies and trajectories. Moreover, we showed that ''nonsequential'' means ''within half an optical cycle,'' and that NSI is not an essentially quantum-mechanical effect. We showed that, in the frequency and pulse duration regime under consideration, SAE ionization yields are in poor agreement with the exact results. TDDFT reproduces the total ionization probability very well, even for the simplest effective potential available, namely, the Hartree-potential. TDDFT fails if one claims physical relevance for the Kohn-Sham orbitals by separately constructing single- and double-ionization yields. However, since generally only the knowledge of the total electron density is necessary, e.g., for calculation of high harmonics generation, TDDFT should produce very accurate results [17].

ACKNOWLEDGMENTS

The author would like to thank P. Mulser and R. Schneider for helpful discussions. This work was supported by the European Commission through the TMR Network SILASI (Super Intense Laser Pulse-Solid Interaction), No. ERBFMRX-CT96-0043.

[1] S. Augst, D. D. Meyerhofer, D. Strickland, and S. L. Chin, J. Opt. Soc. Am. B **8**, 858 (1991).
[2] K. J. Schafer, Baorui Yang, L. F. DiMauro, and K. C. Kulander, Phys. Rev. Lett. **70**, 1599 (1993).
[3] Baorui Yang, K. J. Schafer, B. Walker, K. C. Kulander, P. Agostini, and L. F. DiMauro, Phys. Rev. Lett. **71**, 3770 (1993).
[4] D. N. Fittinghoff, P. R. Bolton, B. Chang, and K. C. Kulander, Phys. Rev. Lett. **69**, 2642 (1992).
[5] P. B. Corkum, Phys. Rev. Lett. **71**, 1994 (1993).
[6] B. Walker, B. Sheehy, L. F. DiMauro, P. Agostini, K. J. Schafer, and K. C. Kulander, Phys. Rev. Lett. **73**, 1227 (1994).
[7] Andreas Becker and Farhad H. M. Faisal, J. Phys. B **29**, L197 (1996).
[8] D. G. Lappas, A. Sanpera, J. B. Watson, K. Burnett, P. L. Knight, R. Grobe, and J. H. Eberly, J. Phys. B **29**, L619 (1996).
[9] J. B. Watson, A. Sanpera, D. G. Lappas, P. L. Knight, and K. Burnett, in *Multiphonon Processes 1996*, edited by P. Lam-

bropoulos and H. Walther, Inst. Phys. Conf. Proc. No. 154 (Institute of Physics and Physical Society, Bristol, 1997), p. 132.
[10] J. Parker, K. T. Taylor, C. W. Clark, and S. Blodgett-Ford, J. Phys. B **29**, L33 (1996).
[11] K. C. Kulander, Phys. Rev. A **36**, 2726 (1987).
[12] K. C. Kulander, Phys. Rev. A **38**, 778 (1988).
[13] M. S. Pindzola, D. C. Griffin, and C. Bottcher, Phys. Rev. Lett. **66**, 2305 (1991).
[14] M. S. Pindzola, P. Gavras, and T. W. Gorczyca, Phys. Rev. A **51**, 3999 (1995).
[15] M. S. Pindzola, F. Robicheaux, and P. Gavras, Phys. Rev. A **55**, 1307 (1997).
[16] E. K. U. Gross, J. F. Dobson, and M. Petersilka, *Density Functional Theory of Time-Dependent Phenomena*, Topics in Current Chemistry, Vol. 181 (Springer, Berlin, 1996), p. 81.
[17] S. Erhard and E. K. U. Gross, in *Multiphoton Processes 1996* (Ref. [9]), p. 37.
[18] C. A. Ullrich, S. Erhard, and E. K. U. Gross, in *Super Intense Laser Atom Physics IV*, Proceedings of the NATO Advanced Research Workshop, Moscow, 1995, Vol. 13 of *NATO Advanced Study Institute Partnership subseries 3: High Technology*, edited by H. G. Muller and M. V. Fedorov (Kluwer, Dordrecht, 1996), p. 267.
[19] C. A. Ullrich and E. K. U. Gross, Comments At. Mol. Phys. **33**, 211 (1997).
[20] D. A. Wasson and S. E. Koonin, Phys. Rev. A **39**, 5676 (1989).
[21] P. B. Lerner, K. J. LaGattuta, and J. S. Cohen, Phys. Rev. A **49**, R12 (1994).
[22] P. B. Lerner, K. J. LaGattuta, and J. S. Cohen, J. Opt. Soc. Am. B **13**, 96 (1996).
[23] P. B. Lerner, K. J. LaGattuta, and J. S. Cohen, Laser Phys. **3**, 331 (1993).
[24] C. A. Ullrich, U. J. Gossmann, and E. K. U. Gross, Phys. Rev. Lett. **74**, 872 (1995).
[25] J. Javanainen, J. H. Eberly, and Qichang Su, Phys. Rev. A **38**, 3430 (1988).
[26] D. R. Schultz, C. Bottcher, D. H. Madison, J. L. Peacher, G. Buffington, M. S. Pindzola, T. W. Gorczyca, P. Gavras, and D. C. Griffin, Phys. Rev. A **50**, 1348 (1994).
[27] R. Grobe and J. H. Eberly, Phys. Rev. A **48**, 4664 (1993).
[28] D. Bauer, Phys. Rev. A **55**, 2180 (1997).
[29] M. D. Feit, J. A. Fleck, Jr., and A. Steiger, J. Comput. Phys. **47**, 412 (1982).
[30] R. M. Dreizler and E. K. U. Gross, *Density Functional Theory* (Springer, Berlin, 1990).
[31] Erich Runge and E. K. U. Gross, Phys. Rev. Lett. **52**, 997 (1984).
[32] Sydney Geltman, Phys. Rev. Lett. **54**, 1909 (1985).
[33] S. Geltman, J. Phys. B **21**, 47 (1988).
[34] Maciej Lewenstein, Kazimierz Rzążewski and Pascal Salières, in *Super-intense Laser-Atom Physics*, Vol. 316 of *NATO Advanced Study Institute Series B: Physics*, edited by B. Piraux, A. L'Huillier, and K. Rzążewski (Plenum, New York, 1993), p. 425.